ORIGINAL ARTICLE

Characterization and optimization of the hydroforming process of AISI 316L steel hydraulic tubes

Alessandro Colpani [1] · Antonio Fiorentino [1] · Elisabetta Ceretti [1]

Abstract
Hydroforming is a metal forming technology that enables the fabrication of complex parts in a low cycle time. The process is based on the plastic deformation of a blank sheet using a pressurized fluid. This paper focuses on the design of a tube hydroforming (THF) process to replace the current cut-and-weld practice for components produced by a company. Specifically, the study focuses on the characterization and optimization of the THF process for stainless steel T-joint parts produced in two sizes: small and large. The new production must improve the final components' quality and maintain the technical requirements of the previous one, especially in terms of the parts' geometry (in particular, the third branch minimum height and thickness) and material (AISI 316L), with competitive production costs. Accordingly, the process optimization is performed in three sequential steps. Initially, the process is characterized by the material flow stress and the friction between a tube and die. Subsequently, this information is used to develop a finite element method (FEM) model, which is validated based on experimental data. The FEM is used to optimize the process parameters (pressure, stroke, and trust force of the counterpunch) to improve the final component quality and guarantee the specific dimensional requirements. Finally, further improvements of the process are implemented (initial precrash of the tube, optimal length of the blank tube, and calibration pressure to avoid wrinkles in the final component). After the THF process optimization, emphasis is placed on the punch geometry. A study is conducted to avoid stress concentrations that may cause punch breakage. The results of this study allow the minimization of tube thinning during the hydroforming process, and guarantee the target value for the third branch height with minimal material consumption. Moreover, the evaluation of different geometrical alternatives allows the stresses acting on the punches to be reduced by 45%.

Keywords Hydroforming · Tube · FEM · Optimization · Die stress · Process design

1 Introduction

Hydroforming (HF) is a manufacturing process characterized by the plastic deformation of a blank using a pressurized fluid that expands the blank in a hollow die to obtain the desired shape [1]. HF is known as sheet hydroforming (SHF) when a sheet blank is deformed, and tube hydroforming (THF) when a tube is processed [2]. In THF, a tubular blank is placed between two die halves and plastic deformation is obtained by two punches that are moved during the process to push the tube edges and feed the material toward the expansion zones. Additionally, pressurized liquid is injected through one punch, thereby expanding the tube [3]. The pressure system comprises a pump, control valves, and an intensifier, while axial hydraulic plungers are used to feed the material into the expansion regions to avoid pressure losses [4]. To guarantee die closure when pressure is increased, hydraulic presses or clamping systems are used [5]. During the process, the die parts must withstand high stresses caused by the high pressure levels and axial loads [6]. Moreover, an adequate die–tube interface is required to minimize friction [7].

THF is a metal forming process that enables tubes to be fabricated with complex sections and shapes [8]. Compared with other conventional tube forming processes, THF is characterized by tooling and assembly cost reduction, fewer

✉ Alessandro Colpani
a.colpani003@unibs.it

Antonio Fiorentino
antonio.fiorentino@unibs.it

Elisabetta Ceretti
elisabetta.ceretti@unibs.it

[1] Department of Mechanical and Industrial Engineering, University of Brescia, via Branze 38, 25123 Brescia, Italy

secondary operations and less waste [9], part weight reduction (through more efficient section designs), and improved final part quality, mechanical properties (enhanced structural strength, stiffness, and surface finish) [10], and dimensional accuracy [11]. The effectiveness in the realization of complex parts and the lower lead time render this technology suitable in several fields, such as automotive [12], fluid delivery, aircraft, structural component manufacturing [13], nozzle production, and home appliances [14].

Tube geometry, material properties, combination of axial feeding and internal pressure, and friction between workpiece and die are parameters that primarily affect THF results [15]. In particular, friction is a fundamental factor in THF technology [16] because of the high contact areas and pressure levels involved in the process, which can retain material sliding. In fact, high friction stresses act on the tube walls, and the material hardly flows to the expansion zones, thereby affecting the part formability and the final component soundness and geometry [17]. When the friction coefficient at the interface between the tube and die is low, the stresses acting on the tube walls are more uniform because of a more uniform friction distribution. As the tube deformation depends on the stresses, the final thickness is significantly affected by friction [18]. Because THF is affected by a large number of parameters, the process can be preliminary investigated using finite element method (FEM) models to evaluate its sensitivity on the process parameters and to optimize it. The friction at the tube–die interface and the material flow stress are key inputs in FEM simulations for THF processes. An effective testing method for the estimation of the tube flow stress law is the tube Bulge test, which, compared with the uniaxial tensile test, can induce a stress state that is closer to that occurring in actual THF process [19, 20].

Furthermore, one recent trend in this field is the development of hybrid manufacturing processes to manufacture metal–polymer components in a single operation [21]. During these processes, a sheet blank is shaped inside a specialized tool using polymer melt pressure as the pressurized fluid [22]. Despite all the benefits of these new-age manufacturing techniques, such as reduction in cycle time, equipment, and production effort, the integration concept increases the complexity of the processes, which requires particular attention when performing their simulations [23]. Therefore, the correct simulation of the THF process is crucial when a new HF process is developed.

This study was conducted in collaboration with a company that produces parts for pipe plants. The study focuses on the replacement of the current cut-and-weld practice with a THF process for the production of stainless steel T-joints. Because the previous products must be replaced by new ones, the same specifications apply, such as the dimensions and material. Moreover, the new products must be economically competitive; therefore, the constraints must be satisfied by minimizing the part cost (which is primarily due to the blank material cost). Furthermore, the company wishes to convert an entire production line; therefore, the two tubes that correspond to the minimum and maximum sizes, i.e., small and large T-joints (hereinafter small-tee and large-tee), respectively, were considered in this study.

The design and optimization of a new THF process were performed in this study by considering both the part and related constraints. In fact, a large number of process variables (e.g., lubrication, material, pressure, and punch stroke trust force) must be considered along with the constraints of the parts (dimensions) and outer market (production cost and blank tubes availability). As this THF process is completely new and complex, the problem was solved using FEM simulations to reduce the investigation costs. Subsequently, experiments were performed for validation purposes. Moreover, the optimization process was segregated into subtasks to simplify the approach by optimizing smaller subgroups of problems at a time. The subtasks are listed below, while the process optimization flow chart developed and used in this study is presented in Fig. 1.

- Part requirements. A critical analysis of the parts was conducted to identify their requirements in terms of material and geometry.
- Process characterization. This task focused on the tube material (flow stress) and tube–die interface (friction) characterization.
- FEM model. Material characterization results were used to develop a mathematical model to study the process in different conditions. Moreover, the model was validated by experimental results.
- Process optimization. The most crucial process phase for the part feasibility was identified. Subsequently, its sensitivity on the process parameters (pressure, punch velocity, and trust force) was investigated, and an optimal configuration was identified and set for the following tasks. Because the part requirements were not fully satisfied, further improvements were introduced in the process (tube preforming and calibration pressure). Consequently, the part feasibility was achieved.
- Tool optimization. During the experimental tests, the punches showed a premature failure. Therefore, a simulative campaign was conducted to evaluate the stresses acting on the punch. Subsequently, different solutions (punch geometry and lubrication) were tested and compared. The results allowed the stresses acting on the punch to be reduced significantly to increase its life.

The final results demonstrate the effectiveness of the proposed procedure in the development of an optimized THF process in terms of process parameters, configuration, and punch geometry. Moreover, they enabled a list of design rules to be established for THF components' manufacturing.

Fig. 1 Process optimization flow chart
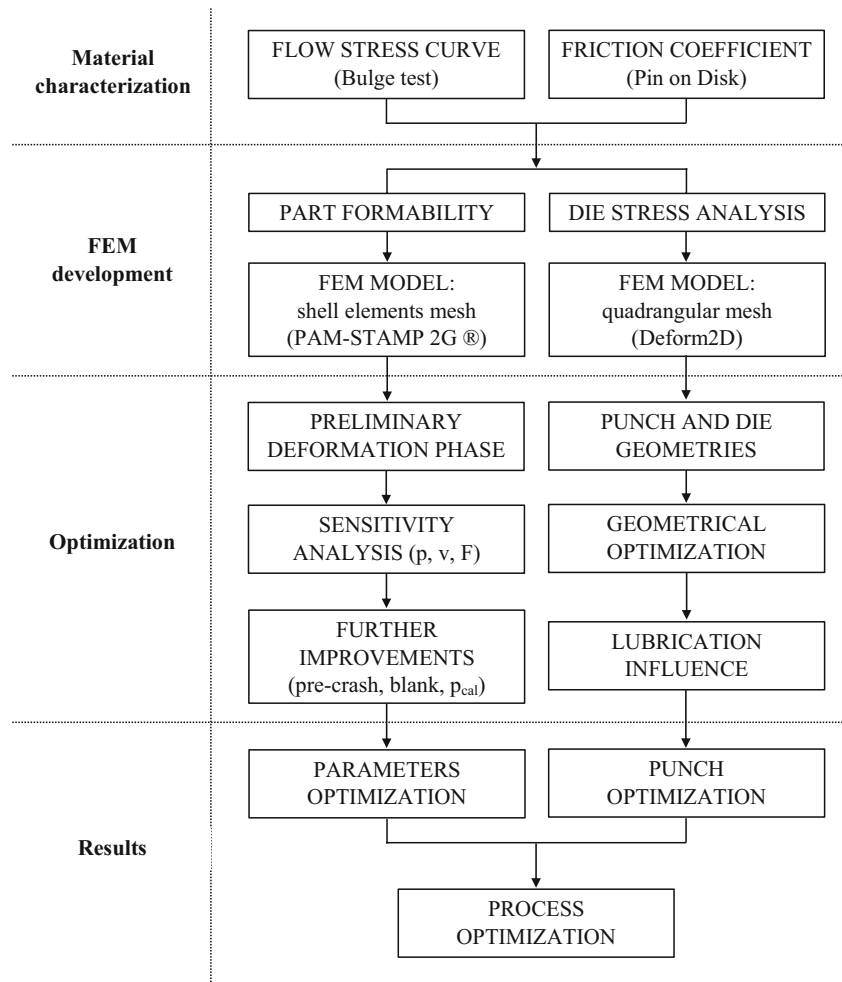
2 Part requirements

The T-joints considered in this study (i.e., small-tee and large-tee) are shown in Fig. 2. To comply with the modular fitting with other components and assembly tools produced by the company, the T-joints must exhibit specifications that represent the main process constraints. In particular, the part must exhibit the minimum overall dimensions (final length L_f and protrusion height H_f). Moreover, the minimum part thickness (w_f) must be guaranteed to accomplish international standards. The geometries of the two parts (dimensional values are classified for nondisclosure reasons) show that the large-tee is 1.5 times larger than the small-tee. These two components are the smallest and largest of a complete production set that the company wishes to fabricate using THF. Further constraints are represented by the blank tube material and the

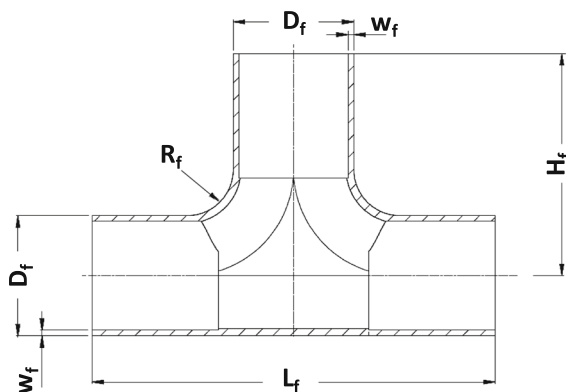|	Small - Tee	Large - Tee
D_f	D	$1.8 \cdot D$
L_f		L
R_f		R
H_f	H	$1.5 \cdot H$
w_f		w_{min}

(normalized values)

Fig. 2 Geometrical requirements for the two tube sizes

dimensions, which are derived based on the final parts' application (water pipes for human consumption) and the company's policies regarding raw material supply. In particular, the tube material must be AISI 316L stainless steel.

3 Characterizations

3.1 Friction

Friction characterization tests were performed using the Pin-on-Disk tribometer (PoD) [24]. Two samples, labeled Pin and Plate (representing mold and tube, respectively) were tested. The Pin was mounted on a guide that moves orthogonally to the Plate, which was mounted on a rotating disk. The Pin and Plate were maintained in contact by a hydraulic cylinder, while the Plate rotated owing to an electric motor controlled in terms of position and velocity. A set of load cells, one placed at the top of the hydraulic cylinder and three positioned under the Pin holder, allowed the detection of the normal force (F) and tangential force (T) acting between the Pin and Plate. Load cell signals were acquired by a data acquisition card and subsequently filtered and processed. The friction coefficient between the Pin and Plate was calculated using the Coulomb relation ($\mu = T/F$).

Tests were performed based on two different contact force (F) levels and lubrication conditions (Table 1). The tested conditions were without lubricant and with the application of Gardomer L6337 (which is the lubricant used by the company). The F force values were set based on the process data provided by the company. The most severe condition and an intermediate condition in terms of operating pressure were selected. Each test was repeated thrice using new Pins and Plates.

The results of the friction tests were compared considering both the average value of the friction coefficient and its evolution during the test to evaluate the variation of friction as a function of lubrication and load. Moreover, the friction uniformity was monitored. Results are reported in Fig. 3. The average values of the friction coefficient are higher in dry tests, where they are dependent on the applied load and not uniform between repetitions. In the tests using Gardomer L6337, the friction coefficient values are lower. Moreover, they do not depend on the load and are highly uniform during
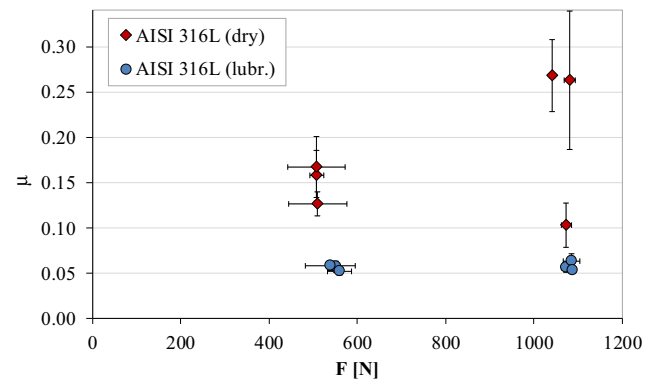

Fig. 3 Friction as function of normal force (with and without lubrication)

the repetitions. Regarding the friction behavior during the single tests (standard deviations in Fig. 3), results show vastly different situations depending on the lubrication condition. In fact, in the dry tests, the friction coefficient is variable (the maximum variability is more than $\pm 40\%$ around the average value, which corresponds to a variability interval greater than $0.153 \div 0.370$). Furthermore, the normal force does not remain constant during the test. These variabilities are related to the nonuniformity of the sample surface. In particular, the variation of the friction coefficient is caused by superficial defects (Fig. 4a), while the variation of the normal force by the nonflatness of the samples. In the tests using Gardomer L6337 (Fig. 4b), both the friction coefficient and normal force are constant and uniform. Because the statuses of the samples used for these tests are the same, the lubricant is used to mitigate the abovementioned tube inhomogeneity.

In conclusion, the use of Gardomer L6337 lubricant results in remarkable improvements in processes related to tube flows. The lubricant enables a uniform friction coefficient of the tube surface to be obtained, which does not depend on the applied load. The average friction coefficient is $\mu_{L6337} = 0.057$.

3.2 Material

Material characterization tests were performed to determine the constitutive law (stress–strain). The material was characterized using the Bulge test, which accurately reproduced the HF process conditions. In fact, in this test, the tube was

Table 1 Friction test parameters

Velocity (mm/s)	Pin area (mm²)	Plate	Force (N)	Pressure (MPa)	Repetitions
3.77	12.56	AISI 316L	500	39.8	3
			1050	83.6	3
		AISI 316L + Gardomer L6337	500	39.8	3
			1050	83.6	3

Fig. 4 Sample surface **a** without and **b** with lubricant

(a)

(b)
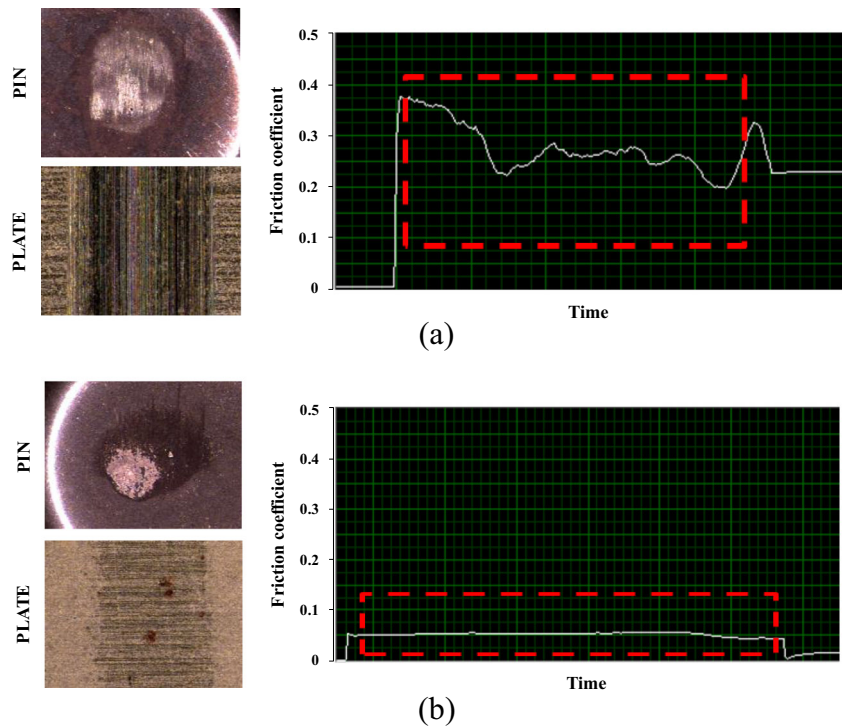
clamped at its edges by a mold and two conical actuators. Subsequently, a pressurized fluid was used to obtain a free expansion of the tube. From an analytical perspective, the Bulge test can be modeled through the membrane theory [19, 20]. During the experimental tests, the maximum pressure value (corresponding to the tube bursting) was determined. Subsequently, the pressure level was gradually decreased to the minimum forming pressure (Table 2).

To determine the material stress–strain curve, the tube maximum expansion zone was identified and marked (Fig. 5a). Subsequently, the circumferential initial and final radii (r_0 and r_θ, respectively), axial radius (r_z), initial thickness (t_0), and final thickness (t) were measured. The initial radius (r_0) was measured from an unformed sample, while the final radius (r_θ) was obtained through bulge height (Δh) measurements at the maximum point (where $r_\theta = r_0 + \Delta h$ at that point). The axial radius (r_z) was measured by acquiring the tube profile using the Mitutoyo QS-200 optical CMM and Eq. (1). The processing procedure was performed using a MATLAB® code written ad hoc to interpolate the tube profile with an ellipse having a semi-axis (b) passing through the maximum expansion area and a semi-axis (a) parallel to the tube axis.

Table 2 Bulge test parameters

Tube AISI 316L	Pressure range
$D \times w_{min}$	$205 \div 410$ bar
$1.8 \cdot D \times w_{min}$	$450 \div 660$ bar

Finally, the tube thickness in the maximum expansion area was measured using a centesimal caliper with round tips.

$$r_z = \frac{a^2}{b} \tag{1}$$

The collected data were used for the calculation of equivalent stress and strain in the material according to von Mises equations. The stress and strain values for the two tested tubes are shown in Fig. 5b. As the flow laws between the small- and large-tee were the same, the datasets were merged and interpolated through the Kuprowsky Eq. (2), which enables the material yield strength corresponding to $\varepsilon = 0$ to be calculated, i.e., 453 MPa.

$$\sigma = 1553 \cdot (\varepsilon + 0.159)^{0.634} \tag{2}$$

3.3 FEM model: THF

The data collected in the experiments for friction and material characterizations were used for the development of an FEM model for the HF process. Subsequently, the experimental final thickness of the components and that obtained with the FEM model was compared to validate the process. The model was developed using the PAM-STAMP 2G ® code and an explicit solver. The following aspects were considered for the model development.
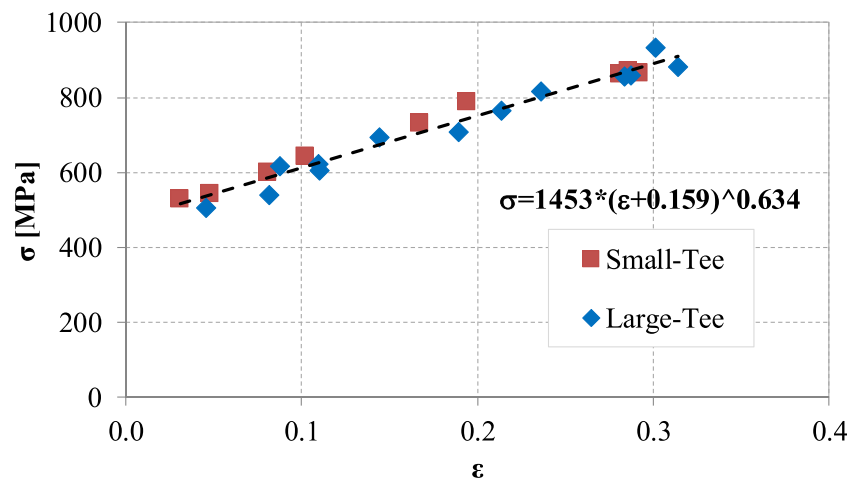
Fig. 5 Bulge test. **a** Maximum expansion area and thickness trend. **b** Stress–strain curve obtained by the test

(a)

$$\sigma = 1453 * (\varepsilon + 0.159)^{0.634}$$

■ Small-Tee

◆ Large-Tee
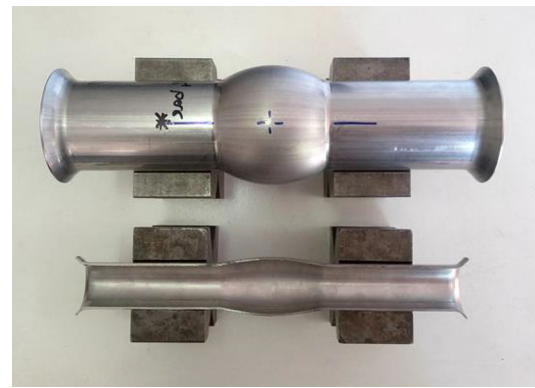
(b)

- Material. The material was modeled using the Eq. (2) obtained from the Bulge test (Fig. 5).
- Geometries. Punch and mold geometries were obtained from the technical drawings supplied by the company. Moreover, the blank tube had a thickness equal to the minimum thickness required by the final part ($w = w_{min}$) and a diameter that was initially lower than the mold diameter ($\Delta\varnothing = -1.4$ mm). During the optimization, the tube diameter was changed and set equal to the die diameter ($\Delta\varnothing = 0$ mm).
- Friction. According to the process specifications, the tube was lubricated with Gardomer L6337 in the expansion area, while the opposite area was characterized by a dry contact. The friction coefficient was set as 0.057 and 0.2 for the lubricated and dry zones, respectively.
- Calculation time. The tube membrane was modeled with two-dimensional (2D) shell elements, and the software simulated the third dimension (thickness) from the volume constancy of each shell. Hence, the model could be simplified from a volumetric (three dimensional) to a superficial (locally 2D) problem. The use of the explicit solver within the shell elements enabled the calculation time to

be reduced considerably. Finally, to further simplify the model, an adaptive remeshing strategy was applied for the tube mesh to locally refine the mesh where necessary. Finally, the model resulted in a calculation time of 2÷4 h for each simulation.

- Process curves. Pressure, stroke, and punch force values were provided by the company (trends are reported in Fig. 6).
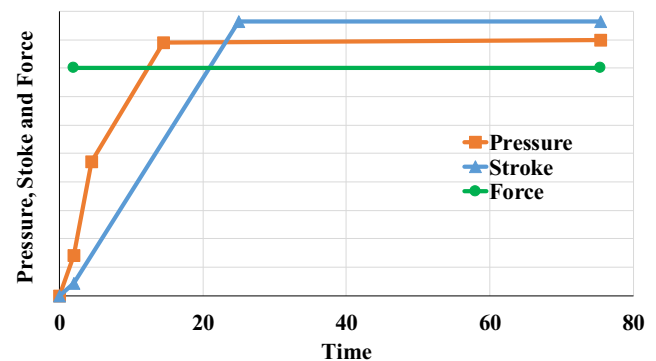

Fig. 6 Process curves (trends)

The model was validated by comparing simulations and experimental samples. In particular, the hydroformed tube thickness was evaluated (Fig. 7). The comparison was performed considering the tube profile along the expansion (A and B in Fig. 7) and sliding (C in Fig. 7) sides. Results (Fig. 8) indicated a good agreement along the A zone (third branch) of the expansion side, with a slight overestimation in the external areas B, where the FEM model calculated a greater material accumulation compared with the experimental samples. This was due to a difference in the external form of the punch used for the model when compared with that used in the experimental texts. As the zone of interest for this process was the expansion area A, and considering that the model precisely matched the experimental results in this zone, the slight discrepancy mentioned above did not increase. Furthermore, along the sliding side C, the FEM model effectively estimated the thickness, while slight differences were observed at the tube ends (D in Fig. 7). For example, the experimental data indicated a higher localized thickening compared with the FEM model. In general, the model accurately predicted the thickness of the hydroformed component, especially in the A zone of the expansion area, which was the most relevant for this process.

The model, which is globally stable and can accurately predict the hydroformed tube geometry, demonstrated some instabilities when the tube was primarily compressed (e.g., at the largest blank tube lengths). Mesh instabilities occurred in the contact areas between the tube and punches (Fig. 9a), and an excessive mesh thinning occurred in the tube central zone (Fig. 9b). Therefore, the developed model was refined to achieve better performances.

Both problems are related to an excessive reduction of the mesh size, which becomes lower than the model stability limit (75% of the shell thickness) [25]. The element size is reduced by the internal remeshing algorithm and the compression stresses acting on the tube during the deformation. These phenomena become critical in the two areas highlighted in Fig. 9 because the material is subjected to a strong axial compression, which reduces the mesh size in this direction. Furthermore, the component is subjected to a significant thickening, especially near the tube–punch contact zone and the stretching along the third branch direction.

A stable solution was identified to enhance the model stability. An initial mesh characterized by large elements along the tube axis (10 mm) and shorter along the circumferential direction (subtended angle of 6°) was used (Fig. 10). Moreover, element remeshing was prevented (refinement = 1). This strategy enabled the excessive axial compression of the mesh to be compensated without losses in the axial discretization of the blank tube. Furthermore, the denser discretization along the tube circumference guaranteed an adequate approximation along its curved surface.

However, this strategy resulted in an extremely coarse mesh for modeling the third branch expansion. In fact, the mesh was stretched and the tube geometry was curved along all directions in this area. This situation resulted in a poor simulation accuracy. Therefore, because the third branch was not affected by model instabilities, remeshing was allowed (refinement = auto; smallest radius to catch = 1 mm) in the tube core to enhance the discretization accuracy. A virtual object (shown in Fig. 10) was introduced. This object and the tube shared the subset of elements that flowed in the third

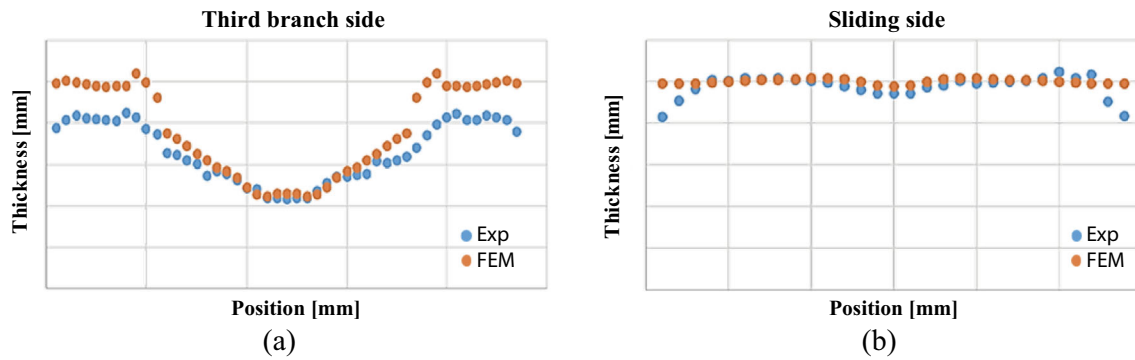**Fig. 7** Final thickness trend
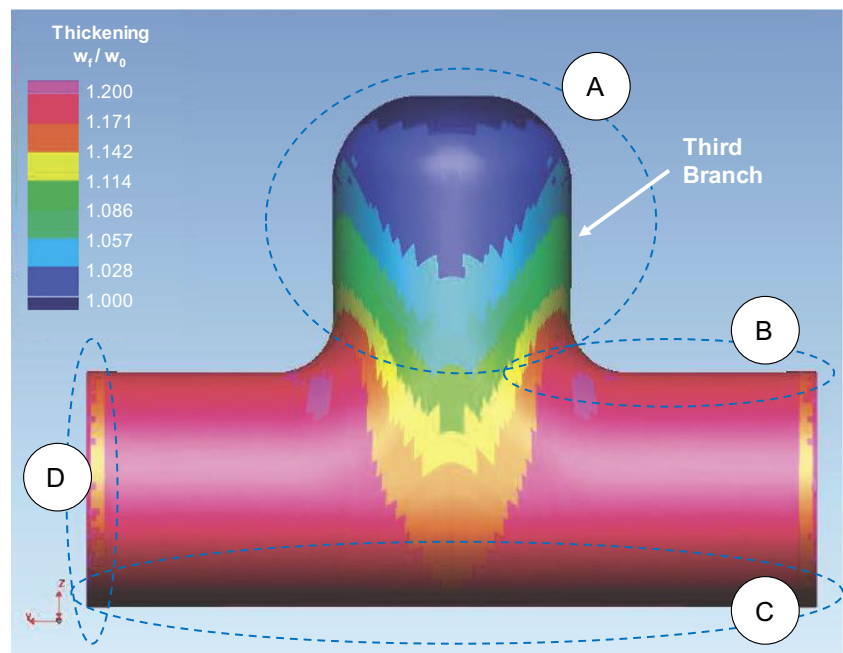
Fig. 8 Comparison of final thickness between simulations (FEM) and experimental samples (Exp) for **a** expansion and **b** sliding sides of the tube

branch. These elements exhibited the same properties except that they could be remeshed by the FEM. Therefore, a local meshing strategy was adopted to guarantee a suitable discretization of the tube in different zones by avoiding numerical instabilities.

4 Process optimization

A simulation was performed to determine the most significant factors affecting the process. Initially, the preliminary phase of the process was identified as the most critical for the part feasibility. Therefore, this specific phase was analyzed to evaluate its effects on the final part characteristics (especially the thickness). Subsequently, a sensitivity analysis was performed for the main process parameters (pressure, punch velocity, and trust force acting on the third branch zone). The results obtained by the FEM simulations enabled a base configuration that was used in a new simulation to be defined to optimize further aspects of the process (such as the precrash phase, initial tube length, and calibration pressure).

4.1 Preliminary phase

A simulation was performed to evaluate the evolution of the tube thickness during the process (Fig. 11). A general tube

wall thickening was observed except for the third branch zone where the tube thinned. Moreover, tube thinning occurred in the initial phases of the process (Fig. 11(a), steps a–d); subsequently, it remained almost constant until the process ended (Fig. 11(a), steps e–i). Therefore, it is necessary to improve the process in the initial phases to limit tube thinning. Furthermore, the final thickness distribution (Fig. 11(a), step i) shows that the most critical geometrical requirement for these components (Fig. 2) is H_f, as it is the height of the third branch zone and has the minimum thickness (w_{min}). Therefore, H_f is related to dome thinning.

In the analyses, it was observed that the company adopted blank tubes characterized by a diameter that was smaller than that required for the final component; the tube diameter required an expansion of 1.4 mm to attain the final component diameter. This expansion was performed at the start of the process as the inner pressure increased. Consequently, the tube thickness reduced initially, which negatively affected the final component.

Therefore, the reduction in thinning by avoiding the initial expansion was evaluated. Owing to the company's policies, the suitable commercial tubes were limited by the raw material supply. For instance, the tube closest to the final part geometry had a diameter that was 0.1 mm lower. The results (Fig. 11(b)) show that the tube initial thinning reduced from 20 to 9% by avoiding the initial expansion (i.e., using a tube with a
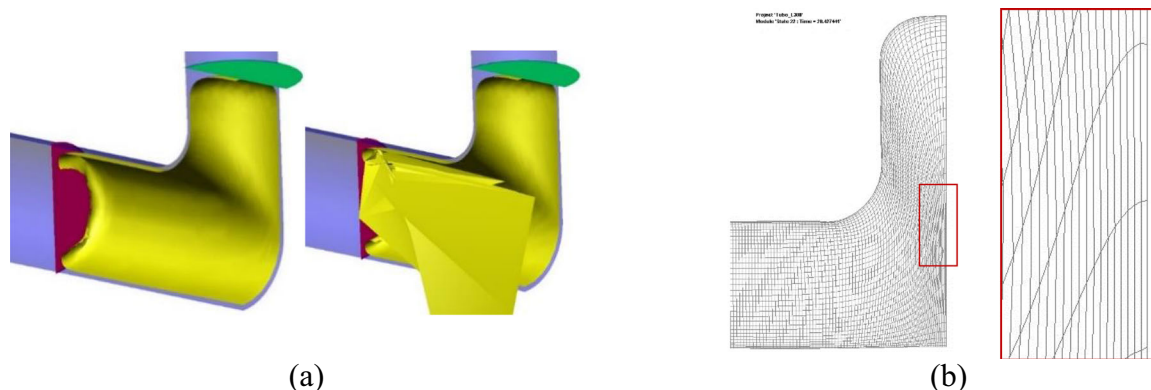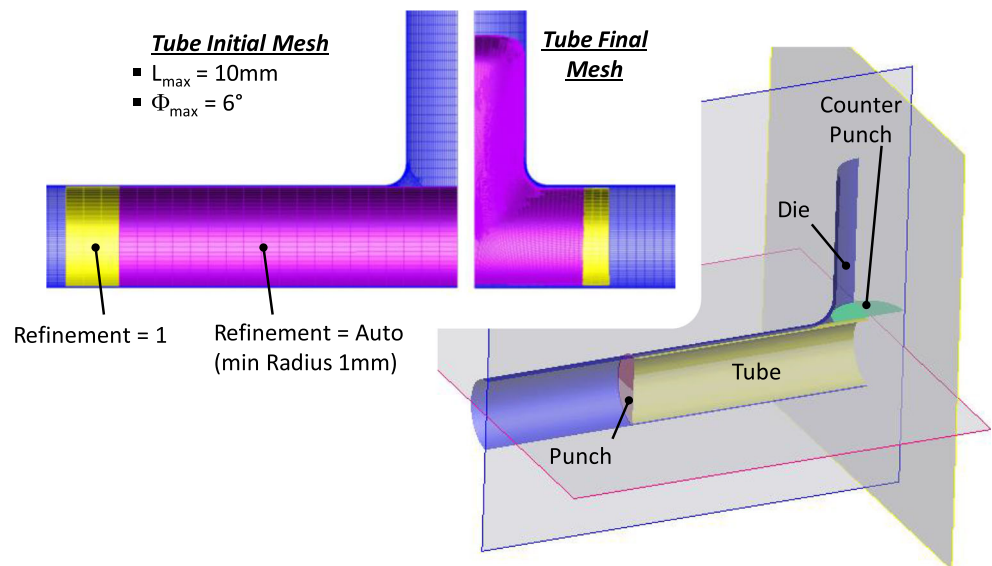

Fig. 9 FEM model instabilities **a** in the area of tube–punch contact (mesh collapse) and **b** in the central zone of the tube (excessive mesh stretching)

Fig. 10 Meshing strategy adopted to avoid calculation instabilities

Tube Initial Mesh
- L_{max} = 10mm
- Φ_{max} = 6°

Tube Final Mesh

Counter Punch

Die

Tube

Punch

Refinement = 1

Refinement = Auto (min Radius 1mm)

diameter equal to the die diameter). The larger diameter of the part requires the excessive material to be removed during the machining phases that follow HF. The presence of sufficient material stock for this machining phase was guaranteed by the significant thickening achieved by the tube during the process (Fig. 11(a)). Therefore, this blank diameter was identified as the most suitable and, accordingly, it was adopted for the remaining investigation.

4.2 Sensitivity analysis and process improvements

This section focuses on the sensitivity analysis and process improvements. The FEM model was used to evaluate the effects of the process parameters (pressure, punch velocity, and trust force) on the most critical requirements of the final part (e.g., H_f). The pressure range was defined by the minimum pressure required to expand the tube and the maximum pressure sustainable by the tube without bursting. Velocity and

force values were selected according to the company's requirements.

The scheme of tested process parameters selected according to the *central composite design* (values are coded for non-disclosure reasons) is shown in Fig. 12. Simulations were performed for both the small-tee and the large-tee.

Small-tee Results showed that the third branch height (H_f) was affected by the pressure value (Fig. 13a). Further, the pressure imposed a stretching effect on the part walls, which was more remarkable where the walls were thinner (i.e., near to the third branch dome). Moreover, as the pressure increased, the dome expanded and pulled the material from the neighboring areas. The expansion occurred only at zones characterized by a thickness close to w_{min} and did not affect other areas (Fig. 13b). Therefore, H_f was maximized at a low operating pressure. Regarding the other tested parameters, the punch velocity and trust force did not significantly affect the part
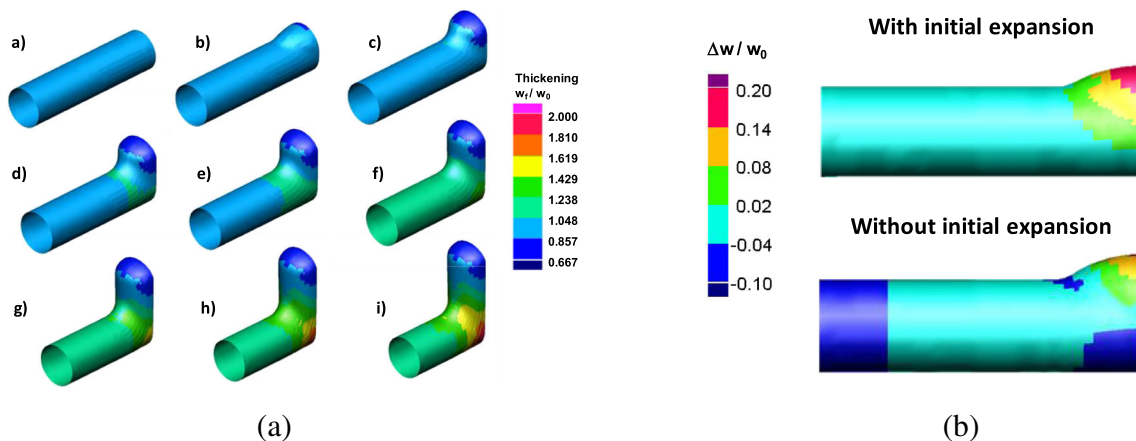

Thickening w_f / w_0

| 2.000 |
| 1.810 |
| 1.619 |
| 1.429 |
| 1.238 |
| 1.048 |
| 0.857 |
| 0.667 |

$\Delta w / w_0$

| 0.20 |
| 0.14 |
| 0.08 |
| 0.02 |
| -0.04 |
| -0.10 |

With initial expansion

Without initial expansion

(a)　　　　　　　　　　　　　　　　　　　　　　　(b)

Fig. 11 (a) Evolution of the component thickness during the process. (b) Thinning reduction with and without the initial expansion phase
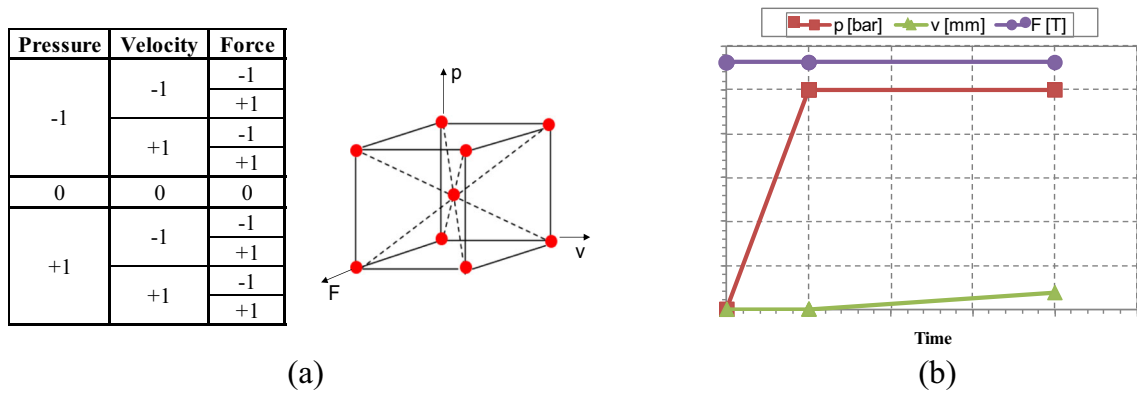
Fig. 12 Sensitivity analysis. **a** Process parameters considered. **b** Process curve (trends)

feasibility. Consequently, a higher punch velocity could be adopted to reduce the HF cycle time (and simulation run time). The trust force was set to the intermediate value.

Large-tee The analysis on the second component (shown in Fig. 14) confirmed that only the pressure affected the process. Therefore, it is better preferable to use a low operating pressure to improve the H_f.

4.3 Further improvements

Despite previous process parameter optimizations, part feasibility was not achieved, and the minimum H_f was not obtained. Therefore, further tests were conducted to enhance the process. In this regard, two strategies were adopted. The first one focused on reducing the initial tube thinning that, as previously shown, was determined by the deformations occurring initially on the tube. The following strategy focuses on the increase in the third branch by feeding more material, which is regarded as last option as it involves the use of more material and hence increases the production costs (specifically the rough material cost).

The enhancements described above enabled the part feasibility to be increased; however, they also increased the risk of tube wrinkling in the large-tee part. Therefore, the pressure curve of the process was modified to reduce the risk of defects.

Precrash Tube preforming is a solution used in HF processes to enhance the formability in areas requiring large expansions. It is based on a local deformation of the tube that is performed to distribute the material to ease the subsequent forming phases of the process [26, 27].

In this study, this technique was applied in the third branch zone as an initial crushing of the tube (precrash) to push the tube material against the die (Fig. 15). The precrash was performed during the initial plasticization phase using a convex counter punch. The effects of precrash on part thickness are shown for the small-tee component in Fig. 16, and similar results were obtained for the large-tee. The total height did not change, while H_f improved for both components. In fact, the H_f value was similar to the dome height, and almost the entire part height satisfied the thickness requirements ($w \geq w_{min}$). Even if the target H_f value was not obtained, the process could effectively distribute the tube material on the final part.
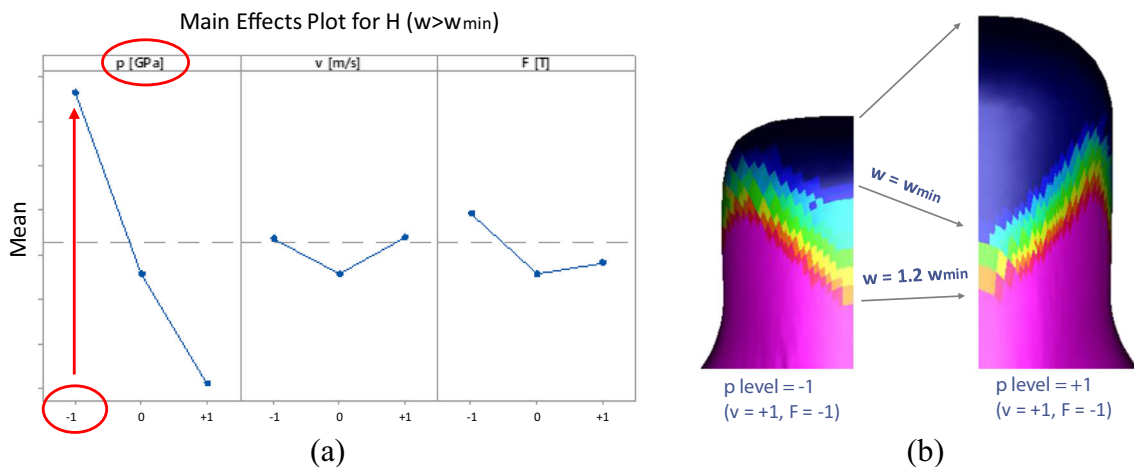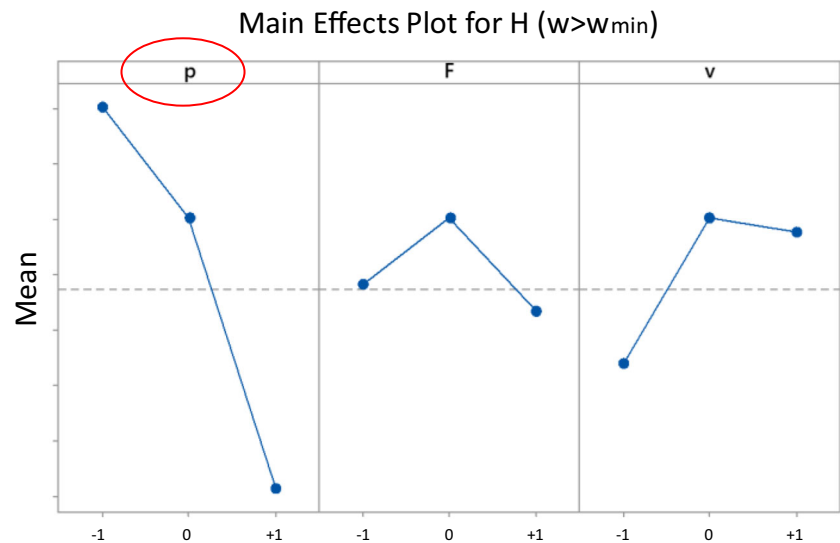

Fig. 13 Small-tee component. **a** Effect of process parameters on H. **b** Stretching effect on the tube walls when the pressure increases

Fig. 14 Large-tee component: effect of process parameters on H

Main Effects Plot for H (w>w_{min})

Optimal initial length of the tube (L_0) The described enhancements enabled almost the entire third branch to reach the thickness requirement ($w \geq w_{min}$) (Fig. 16). Therefore, this process configuration is more efficient in terms of material distribution, and it can be used to investigate the possibility of lengthening the blank tube to reach the target H_f. Simulations were performed using different tube initial lengths (L_0). The third branch height (H) obtained in the simulations is shown in Fig. 17 for the small-tee component.

It can be observed that H increased linearly with L_0. Furthermore, the low slope of the regression line indicates that only a small fraction of the material can reach the third branch area. The ratio between the increases in branch height and tube length is 1:7, while the remaining material accumulates in the feeding walls (B and C areas in Fig. 7). Using the results in Fig. 17, the appropriate L_0 value for obtaining H_f can be estimated. The same procedure was adopted to estimate the optimal initial length of the blank tube for the large-tee part. Similar results were obtained; however, wrinkle defects appeared on the part when longer tubes were adopted ($p_{cal} = 0\%$ in Fig. 18a). Therefore, an additional set of simulations was performed to solve the problem.

Calibration pressure (p_{cal}) The appropriate L_0 value for the large-tee component resulted in the formation of wrinkles owing to the higher compression withstood by the tube during the process ($p_{cal} = 0\%$ in Fig. 18a). Therefore, to stabilize the tube and based on previous results, the pressure was maintained low in the early stages of the process (Fig. 11(a), steps a–d) to reduce tube thinning. Subsequently, a higher pressure (p_{cal}) was used for the remaining process (Fig. 11(a), steps e–i) to counteract the formation of wrinkles. The new pressure curve is presented in Fig. 18b; the results (Fig. 18a) show that this solution enables wrinkles to be eliminated. Furthermore, the use of p_{cal} results in an improvement in H_f (Fig. 19). In fact, the pressure increase after the tube thinning does not further affect the dome thinning and facilitated the stretching of walls in the third branch zone, thereby achieving a better material distribution and a larger H_f.

5 Punch geometry optimization

An additional aspect of the THF process that was enhanced in the present study was related to the geometry of the punches that sealed and pushed the tube in its ends (D zone in Fig. 6).
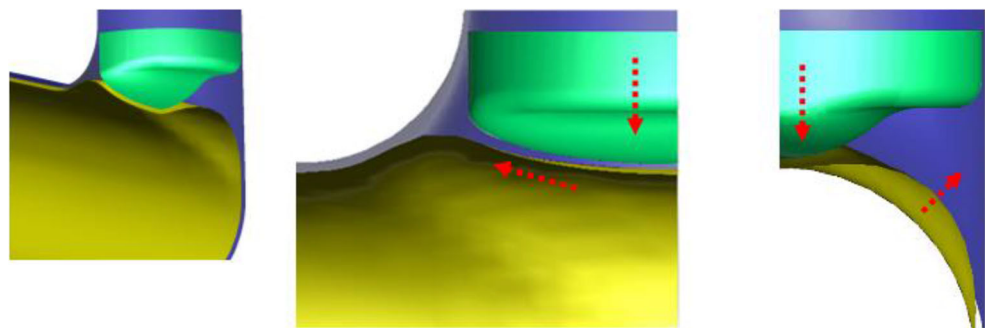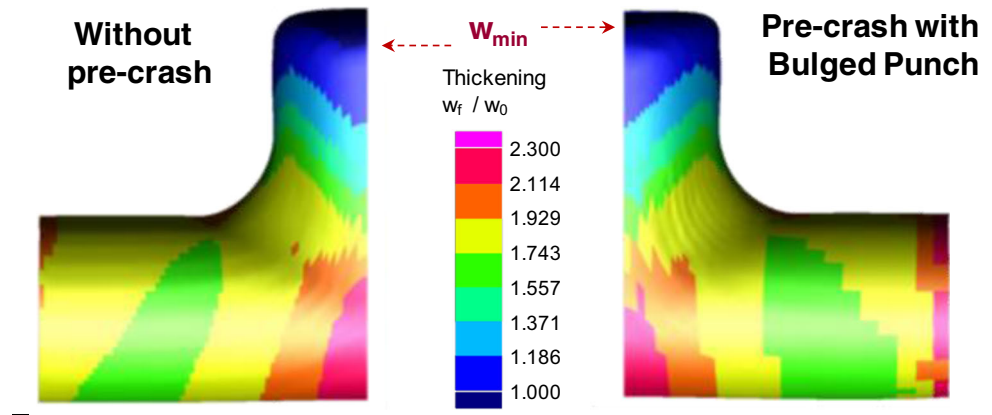
Fig. 15 Material flow during precrash

In fact, some punches (such as those used for the large-tee component production) prematurely broke after a few components were formed. Therefore, an additional FEM model was developed to evaluate the forces acting on the punch and to optimize its geometry to reduce the local stresses.

5.1 Punch breakage

The punch fracture surface (which is ascribable to fragile breakage) is shown in Fig. 20. The fracture starts from the shoulder where the thrust forces of the tube are discharged during the process. The possible breakage causes, which can act in single or combined manner, are the excessive material hardness and stress overload. Because the brittleness of a steel increases with its hardness, the punch resistance can be increased by reducing the material hardness, thereby improving its tenacity. Furthermore, the workloads should be limited to below the resistance limit of the material.

5.2 FEM model: Punch stresses

An FEM model was used to perform a die stress analysis on the punch. The stresses acting on the punch were localized on
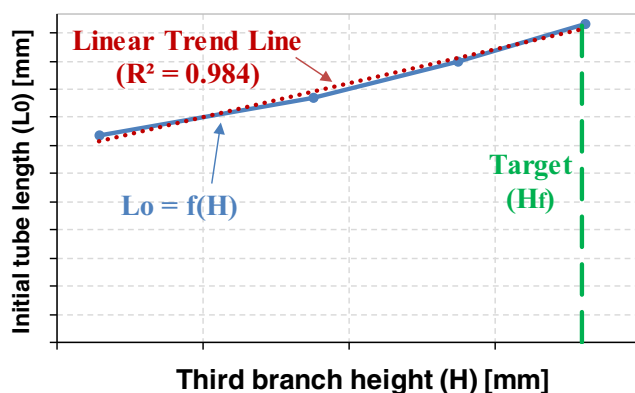

Fig. 17 Small-tee. Trend of the initial tube length (L_0) when the third branch height value (H) increases

a narrow area. Moreover, the tube material underwent a massive deformation in this area.

The previous developed model is based on shell elements that are suitable for studying thin-walled parts with wide surfaces that undergo primarily membrane stretching, as in tube- or sheet-forming processes. Therefore, the previous model is not suitable for the punch stress study.

Hence, a massive FEM model was designed to simulate the local contact between the punch and tube (Fig. 21a). The contact loads depended on the overall compressive force that acted locally on the punch. Therefore, only the resultant compressive force is of interests, while how it is provided by the entire process is negligible. Accordingly, the calculation can be simplified by developing an axisymmetric FEM model based on the on-tube compression without expansion. Moreover, an additional symmetry plane orthogonal to the tube axis was used. The FEM model was developed using Deform2D code (Fig. 21), and the simulation was categorized into two phases:

- Compression up to maximum load. The punch was modeled as a rigid part that compressed the tube with a constant internal pressure and moved with a constant velocity until the axial load value (corresponding to the punch breakage) was reached. The tube was modeled as a massive part, a quadrangular mesh was used, and the element size was 1/17, and the thickness of the punch area was 1/9 in the remainder of the tube. Furthermore, the worst lubrication condition, which was the dry contact in the sliding area (C in Fig. 6), was considered. The geometries, internal pressure values, punch velocity, and maximum load that resulted in the punch breakage were provided by the company. The estimated maximum compression load was 650 kN.

- Die stress analysis. Once the maximum load was attained, the punch and mold were modeled as deformable elastic objects, and the tube was removed and substituted by the contact stresses acting on the punch and mold surfaces.

Fig. 18 **a** Effect of calibration pressure (p_{cal}) on wrinkle elimination. **b** Example of a process curve when the calibration pressure p_{cal} is set (p is the pressure, v the punch velocity, and F the trust force)
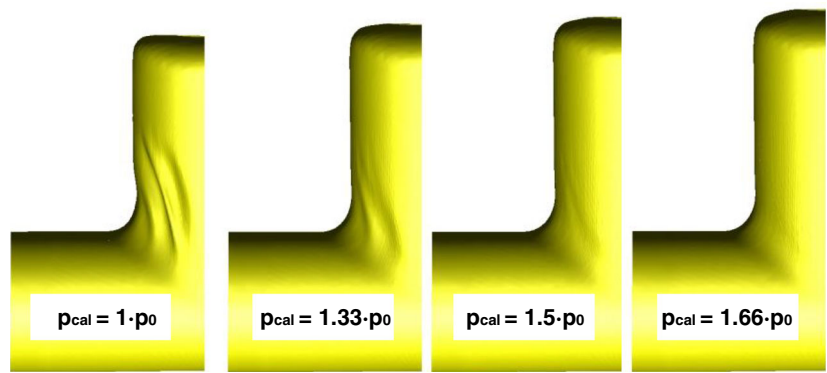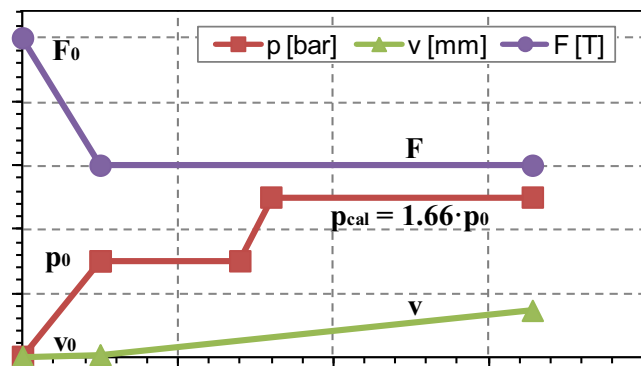
Subsequently, an elastic analysis was performed to estimate the stresses acting on the punch and mold.

The results of die stress analysis for the original geometry of the punch (Fig. 22a) indicated that the mold was less stressed than the punch. The maximum stress was located in the shoulder corner that corresponded to the punch breakage zone. Moreover, these stresses were caused by the bending moment of the resulting forces ($\overrightarrow{R_1}$, $\overrightarrow{R_2}$), which were characterized by high gradients.

5.3 Geometrical optimization

To reduce the stresses acting on the punch, different geometrical variants were considered in a comparative study. The tested geometries were based on the introduction of a discontinuity surface to interrupt the stress propagation within the punch material. The outer geometry of the punch was maintained. Therefore, the punch was categorized into two parts (i.e., upper and lower punches) by a cut surface passing by the punch corner where the highest stresses were located. In
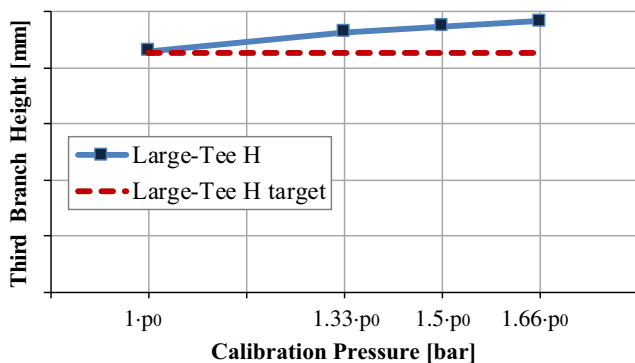

Fig. 19 Effect of calibration pressure p_{cal} on the third branch height H ($w \geq w_{min}$)
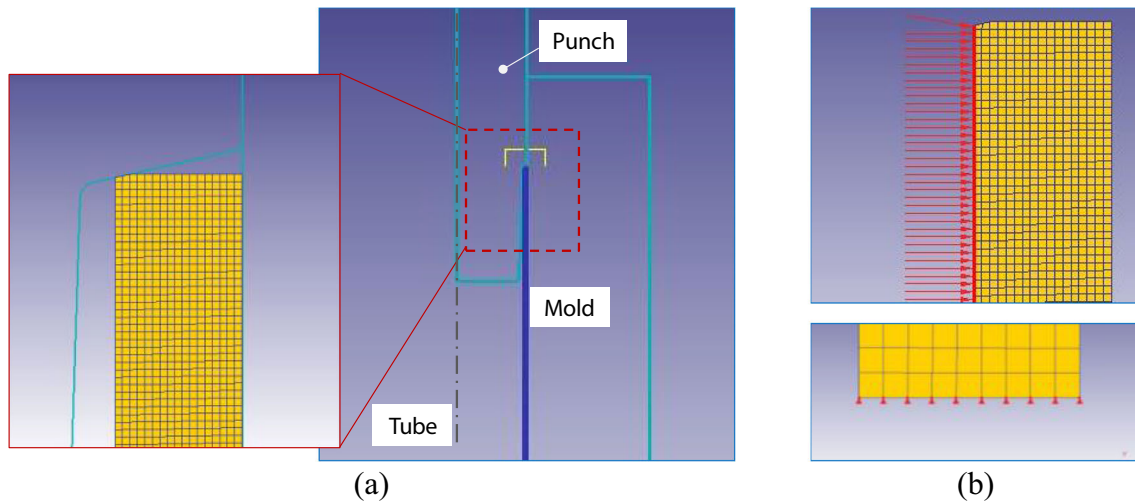

Fig. 20 Punch fracture surface

Fig. 21 Details of the FEM model for the punch study. **a** Axisymmetric model with punch, mold, tube, and details of the mesh. **b** Details of the boundary conditions to simulate pressure (above) and the plane of symmetry (below)

addition, different separation surfaces were tested (Fig. 23). The surfaces were designed to exhibit a chamfered orthogonal profile (a), a 45° profile (b), a combination of the previous profiles (c), and a toroidal profile (d). Finally, the cut surface that provided the best results was tested under optimal lubrication conditions.

Die stress analysis results are compared in Fig. 24 in terms of the maximum stresses acting on the punch (the highest between the upper and lower elements) and mold as the cut surface and lubrication change. In dry conditions ($\mu = 0.2$), the use of a cut surface (A to D in Fig. 24) enabled the maximum stresses acting on all the die zones to be reduced. The B geometry resulted in the best reduction on the punch (− 36%).

Moreover, when a good lubricant was adopted ($\mu = 0.057$), the B geometry enabled a further stress reduction, until almost half of or the initial values (− 45% on the punch and − 51% on the mold). In conclusion, the use of cut planes and a good lubricant effectively reduced the stresses acting on the dies. This corresponds to a reduction in both punch breakage risk and mold wear decrease.

6 Discussion

The results presented herein are summarized in the following list:

Fig. 22 **a** Die stress analysis on the initial punch geometry and **b** scheme of the bending moments
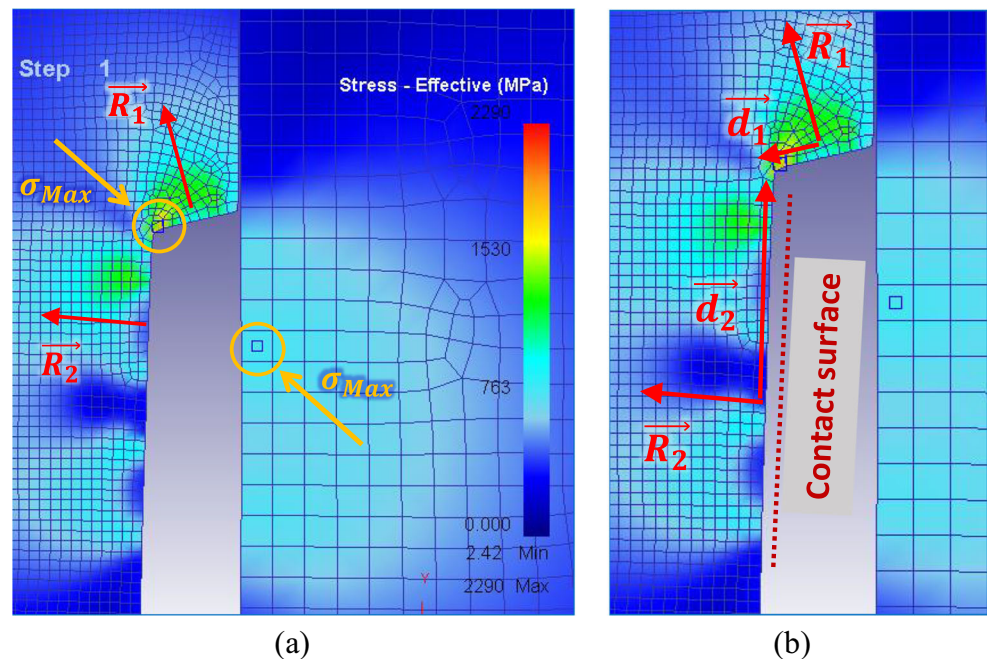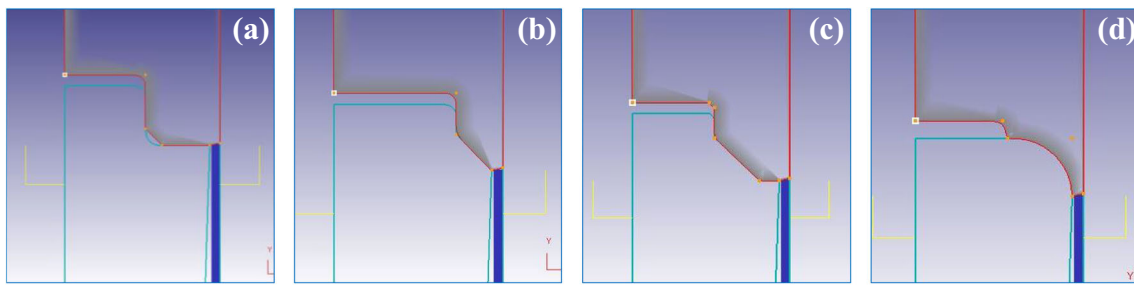
Fig. 23 Tested variants of the punch geometry. **a** A chamfered orthogonal profile. **b** A 45° profile. **c** A combination of the previous profiles. **d** A toroidal profile

- Friction. The use of a lubricant enables a better tube flow and a uniform friction coefficient on the tube surface to be obtained. Therefore, the friction coefficient does not depend on the applied load. These results agree with those in the literature, where it is demonstrated that a low and uniform friction coefficient improves the material slide [15].

- Bulge test. Tests were conducted on tubes characterized by two different diameters. The results show the overlapping of σ–ε curves in the two different cases. In general, different tube diameters undergo different deformations, which results in different residual stresses in the material. The present analysis was conducted on annealed AISI 316L tubes, where thermal treatment removed the stress state. Therefore, when annealing is performed, it is sufficient to test only one diameter. In these cases, it is preferable to test larger tube diameters because of the lower pressure required to expand the material [19, 20].

- FEM model for THF. Shell elements enable the computational time to be reduced; however, their dimensions may be limited by the part thickness. In the THF process, an increase in thickness and a decrease in tube length owing to compression can result in instabilities [28]. Therefore, local meshing strategies should be adopted. An initial mesh characterized by large elements along the tube axis and shorter ones along the circumferential direction was used (Fig. 10). Moreover, element remeshing was

prevented for all the tube zones except for the third branch. This enables numerical instabilities to be avoided and guarantees a suitable tube discretization.

- THF process. The minimum thickness is primarily determined during the preliminary phases of the process (Fig. 11). To reduce tube thinning, it is useful to decrease the pressure at the beginning of the forming process and perform a preforming operation (i.e., precrash). Regarding the main process parameters [29, 30], the pressure should be decreased during the process to decrease material stretching in the free expansion zone. Additionally, it is useful to provide a final pressure increase to avoid the formation of wrinkles [30]. The velocity resulted was not influent with regard to the bulge height; therefore, it should be increased to reduce the cycle time. Finally, the trust force did not affect the third branch height. Therefore, the value of this parameter can be freely set according to other specific requirements.

- Blank material. The THF process for manufacturing T-joints is related to high costs owing to material consumption. Therefore, even if increasing the tube length is effective for attaining the target bulge height, this solution should be the last option to be considered. It is preferable to address the process parameters (especially the pressure curve) and additional operations (especially the precrash).

- *Punch geometry.* The die stress analysis performed on the punch demonstrated that the punches were excessively

Fig. 24 Comparison between the maximum stresses acting on the punch (upper and lower parts) and on the mold as the punch geometry and lubrication change
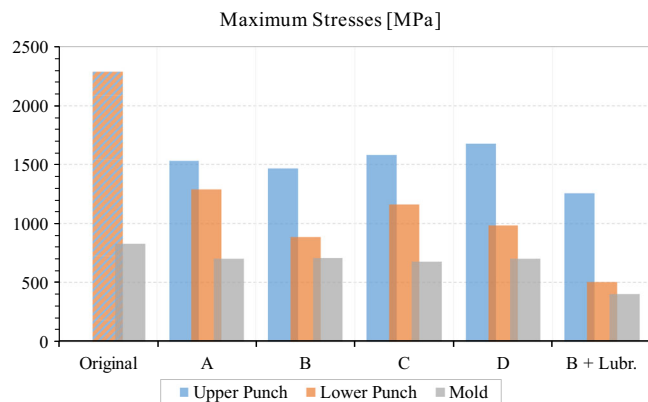
Geometry	σ max variation	
	Punch	Mold
Original	-	-
A	-33%	-15%
B	-36%	-14%
C	-31%	-19%
D	-27%	-15%
B+Lubr.	-45%	-51%

stressed. This situation is ascribable to the punch failure, as the punch breakage zone corresponds to the maximum stress zone in the punch geometry. Therefore, considering the approaches of documented studies [31, 32], different geometrical solutions for the punch were considered. The main differences in the new tested geometries were due to a discontinuity surface that was introduced to interrupt the stress propagation within the punch material. The results in terms of stresses acting on these new punch geometries demonstrate the effectiveness of using cut planes and a good lubrication condition to considerably reduce the stress state and hence the risk of a premature punch failure.

7 Conclusions

The optimization of a tube HF process was presented herein. An actual industrial process was investigated to realize two sizes of AISI 316L T-joints by satisfying the geometrical requirements requested by a company. The investigation was based on two FEM models that were developed to optimize the process parameters and extend the die life. Moreover, as the problem was multivariate, the investigation was divided in subtasks, each optimizing a specific part of the process.

The results of the investigation on the tube HF of AISI 316L stainless steel T-joints can be summarized as follows:

- Lubricant. Gardomer L6337 is a good lubricant as it guarantees a uniform tube slide that is independent of the normal pressure in the range $39.8 \div 83.6$ MPa. Moreover, it enables the stress acting on the punch and mold to be reduced significantly, thereby increasing their life.
- Thickness. The thickness profile on the component dome was determined by the preliminary phases of the process (i.e., when the material initially expanded and entered the T-joint third branch). The thickness in the other areas of the part was determined by the remainder of the process.
- Pressure. A low pressure value was necessary in the preliminary phases to reduce the amount of material flowing in the dome. Once the dome thickness was maintained (i.e., the tube has expanded to fill the circular section of the third branch), a pressure increase stretched the tube material, thereby increasing the third branch height. The high pressure was effective in removing wrinkles in the tube in large axial feeding.
- Preforming. The precrash of the tube performed using a bulged punch enabled the part thickness to be further enhanced.
- Tube length. Increasing the tube length increased the third branch height. However, this was not an efficient solution as the ratio between the increases in height and length was

1:7. As the amount of blank material affected the component cost, the last option was to increase the tube length.
- Punch geometry. Feeding punches were the most stressed die part. The stresses were localized on the shoulder that sealed the tube. The use of a cut surface that interrupted the stress propagation enabled the loads on both the punch and mold to be reduced significantly.

In summary, the systematic approach proposed herein was effective for the optimization of THF processes. This study was performed on T-joint geometries. Although similar conclusions are expected for other geometries, the investigated aspects of the process could affect the final part differently owing to geometry changes. Therefore, future studies will be performed to evaluate the difference between the replaced cut-and-weld process and the new THF process from an economic perspective. Hence, the entire process from the blank preparation to the final testing and shipping will be considered in terms of time, material, and equipment resources.

References

1. Zhang SH (1998) Developments in hydroforming. J Mater Process Technol 91:236–244
2. Han S, Woo Y, Hwang T, Oh I, Moon YH (2019) Tailor layered tube hydroforming for fabricating tubular parts with dissimilar thickness. Int J Mach Tools Manuf 138:51–65
3. Langa LH, Wang ZR, Kang DC, Yuan SJ, Zhang SH, Danckert J, Nielsen KB (2004) Hydroforming highlights: sheet hydroforming and tube hydroforming. J Mater Process Technol 151:165–177
4. Alaswad A, Benyounis KY, Olabi AG (2012) Tube hydroforming process: a reference guide. Mater Des 33:328–339
5. Ahmed M, Hashmi MSJ (1997) Estimation of machine parameters for hydraulic bulge forming of tubular components. J Mater Process Technol 64:9–23
6. Chu GN, Chen G, Lin YL, Yuan SJ (2019) Tube hydro-forging − a method to manufacture hollow component with varied cross-section perimeters. J Mater Process Technol 265:150–157
7. Liu, Z., Lang, L., Ruan, S. et al. Effect of internal pressure assisted on hydroforming for CP800 high-strength steel torsion beam. J Braz. Soc. Mech. Sci. Eng. 41, 90 (2019). https://doi.org/10.1007/s40430-019-1570-9
8. Koç M, Altan T (2001) Overall review of the tube hydroforming (THF) technology. J Mater Process Technol 108:384–393
9. Kim BJ, VanTyne CJ, Lee MY, Moon YH (2006) Finite element analysis and experimental confirmation of warm hydroforming process for aluminum alloy. J Mater Process Technol 187-188:296–299
10. Moon YH, Kim DW, Van Tyne CJ (2008) Analytical model for prediction of sidewall curl during stretch-bend sheet metal forming. Int J Mech Sci 50:666–675
11. Oh SH, Jeon BH, Kim HY, Yang JB (2006) Applications of hydroforming processes to automobile parts. J Mater Process Technol 174:42–55

12. Dohmann F, Hartl C (1996) Hydroforming – a method to manufacture light weight parts. J Mater Process Technol 60:669–676

13. Liu J, Zhang Z, Manabe K, Li Y, Misra RDK (2014) Microstructure evolution in TRIP-aided seamless steel tube during T-shape hydroforming process. Mater Charact 94:149–160

14. Kang BH, Lee MY, Shon SM, Moon YH (2007) Forming various shapes of tubular bellows using a single-step hydroforming process. J Mater Process Technol 194:1–6

15. Fiorentino A, Ceretti E, Giardini C (2013) Tube hydroforming compression test for friction estimation—numerical inverse method, application, and analysis. Int J Adv Manuf Technol 64:695–705

16. Luege M, Luccioni BM (2008) Numerical simulation of the lubricant performance in tube hydroforming. J Mater Process Technol 198:372–380

17. Fiorentino A, Ceretti E, Giardini C (2013) The THF compression test for friction estimation: study on the influence of the tube material. Key Eng Mater 549:423–428

18. Fiorentino A, Marzi R, Ceretti E, Giardini C (2011) Numerical inverse method for friction coefficient estimation in tube hydroforming. Key Eng Mater 473:548–555

19. Hwang YM, Lin YK, Altan T (2007) Evaluation of tubular materials by a hydraulic bulge test. Int J Mach Tool Manu 47:343–351

20. Bortot P, Ceretti E, Giardini C (2008) The determination of flow stress of tubular material for hydroforming applications. J Mater Process Technol 203:381–388

21. Michaeli W, Maesing R (2010) Injection moulding and metal forming in one process step. Prog Rubber Plast Recycl Technol 26(4):155–166

22. Farahani S, Arezoodar AF, Dariani BM, Pilla S (2018) An analytical model for nonhydrostatic sheet metal bulging process by means of polymer melt pressure. J Manuf Sci Eng 140:091010

23. Farahani S, Yelne A, Akhavan Niaki F, Pilla S (2019) Numerical simulation for the hybrid process of sheet metal forming and injection molding using smoothed particle hydrodynamics method. SAE Tech Pap Ser 1:1–8

24. Attanasio A, Fiorentino A, Ceretti E, Giardini C (2007) Experimental device to study surface contacts in forming processes. American Institute of Physics 907:275–278. In: Proceedings of the 10th ESAFORM Conference on Material Forming. 18–20 April 2007, Zaragoza (Spain). https://doi.org/10.1063/1.2729524

25. PAM-STAMP 2G 2018 manual

26. Hu ZJ, Zhang FF, Chen J, Han C (2015) Uniform thickness distribution oriented preforming design of tube hydroforming with rectangular section. J Plast Eng 22(3):92–97

27. Trott, A., & Nikhare, C. P. (2018). Effect of preform during low pressure tube hydroforming. In Advanced Manufacturing (ASME International Mechanical Engineering Congress and Exposition, Proceedings (IMECE); Vol. 2). American Society of Mechanical Engineers (ASME). https://doi.org/10.1115/IMECE2018-86090

28. Guo N, Liu K, Zheng S, Xue K (2019) A systemic study on hydroforming process of exhaust pipe by FE simulation and experiment. Int J Mater Prod Technol 59:34–47

29. Lin SL, Chen ZW, Chen FK (2018) A study on localized expansion defects in tube hydroforming. J Chin Inst Eng 41:149–159

30. Cui XL, Wang XS, Yuan SJ (2019) Effects of mechanical property parameters on wrinkling behavior of thin-walled tubes in hydroforming process. Int J Adv Manuf Technol 100:729–740

31. Mingtao C, Xiaoting X, Jianghuai T, Heng G, Jianping W (2018) Improvement of formability in T-shaped tube hydroforming by a three-stage punch shape. Int J Adv Manuf Technol 95:2931–2941

32. Chen C, Gan Y, Du J, Huang C, Chen Q (2011) FEM simulation and optimization of process parameters for tube hydroforming. Appl Mech Mater 101-102:901–904